Advances in Science and Technology Research Journal

Advances in Science and Technology Research Journal 2023, 17(5), 114–129
https://doi.org/10.12913/22998624/171489
ISSN 2299-8624, License CC-BY 4.0

Received: 2023.07.14
Accepted: 2023.09.23
Published: 2023.10.20

Impact of TIG Welding Parameters on the Mechanical Properties of 6061-T6 Aluminum Alloy Joints

Salah Sabeeh Abed Al Kareem[1], Basma L. Mahdi[1*], Hiba K. Hussein[1]

[1] Department of Automated Manufacturing Engineering, Al- Khwarizmi College of Engineering, University of Baghdad, Bagddad, Iraq

* Corresponding author's e-mail: basma.l@kecbu.uobaghdad.edu.iq

ABSTRACT

The most common gas-shielded arc welding method is tungsten inert gas welding, which uses shielding gas to isolate the welded area. Such technique is mostly used in the industrial domain, including steel framework fabrication and installation, plumbing systems, and other building jobs. The welding method and the implementation of a suitable welding joint based on some factors that contribute to the fusion process were studied in the present research. The research investigated the specifications and efficiency of the area to be welded in terms of the thermal effect on the welding joint shape and some significant mechanical property-related factors which that were determined during the welding process. In this paper, aluminum alloy sheets, AA 6061-T6, with a thickness of 3 mm, were used with a 60mm width and 80mm length. These sheets were prepared to be welded using welding currents of 90A, 95A, and 100A, welding speeds of 60mm/min, 80 mm/min, and100 mm/min, and gas flow rates of 8 l/min, 9 l/min, and 10 l/min. The experiments were designed at three distinct levels. These levels were selected to create the L9 orthogonal array. Regression analysis, signal-to-noise ratio evaluation, and analysis of variance were carried out. The created model has enhanced accuracy by predicting the reinforced hardness found in the weld specimens, according to the regression study, which showed R2= 90.09%. In addition, it was discovered that the ideal welding parameters for a welded specimen were 100 A for welding current, 80 mm/min for welding speed, and 9 l/min for gas flow. The present research examined the shape of the thermal distribution of welded parts using the engineering computer program ANSYS. The experimental results clarified the proposed approach, as they showed that the welding current is the most influential factor in the hardness of the weld using the fusion process of 90.95%, followed by the welding speed of 7.48%, while the gas flow rate of 1.52% has the least effect. The authors recommend using qualified welders to ensure optimal performance. It is anticipated that these findings will serve as a foundation for analysis to optimize welding processes and reduce welding defects.

Keywords: Tungsten inert gas, welding, joint shape, micro hardness, thermal distribution, ANSYS.

INTRODUCTION

Fusion welding is the operation of heating two or more materials to a melting point for joining or integrating them to make one piece. The pressure applied is not required in this operation. The welding rig generates the heat that melt the material surfaces and joins them together. Fusion welding can be classified according to the heat sources. Arc welding is the most common and popular type of fusion welding process it is divided into two types TIG and MIG. For thin plate-like aluminum 6061, the TIG process can be used smoothly and easily. There is a dearth of knowledge regarding TIG welding of aluminum alloys AA6061-T6 in documented literature. Many researchers studied the parameters used in the welding process such as (gas flow rate, axial force, welding current, welding voltage, time used during welding, rotational speed) which have a significant impact on refining grain in the fusion area and weld bead geometry for improving both physical and mechanical behavior of fusion welded joint [1–4]. DOE of the experiment

design is the most effective way in predicting the experiments used in the fusion welding process. Currently, more studies are concentrating with the description of the metal sheet microstructure and the investigation of the mechanical characteristics for similar or dissimilar sheet metal with lap junction, butt joints using friction stir welding (Mic) [5–9], A-TIG welded[10], the use of laser welding [11] and laser-TIG welding. both hybrid & electron beam welding [12, 13]. For instance, considering that weld operations entail the speed rate of the tool, the speed of the weld, the rotational speed, etc.

Various type of optimization method is used to find the relationship between input and output parameters. The most common way for finding the optimal properties is by using response surface methodology (RSM) Taguchi method [14–18]. Adalarasan and Santhanakumar performed welding tests on AA6061-T6 alloy. The alloy is composed of Taguchi orthogonal L9 array. The authors utilizing grey relational analysis to investigate the impact of welding parameter. The input parameters included arc voltage that is ranged (17 V to 24 V), current ranged (160 A to 180 A), welding speed ranged (90 mm/min to 110 mm/min), and gas flow rate ranged (9 lit/h to 14 lit/h). It was discovered that current is more significant than mechanical properties by 47%, followed by arc voltage by 35%, [19].

Khoshroyan and Darvazi [20], [21]used examined the distribution of the heat and remaining stress in aluminum 6061-T6 using ANSYS software, during MIG welding. Fluxes were not used in this study, and the only factors considered were welding speed and current. Meanwhile, Pk et al. [22] focused on enhancing the mechanical properties of TIG-welded aluminum 6061-SiC composite. In this study, fluxes were homogenized and aged at temperatures of 100°C, 150°C, and 200°C. The specimen that had been aged and blended under laboratory circumstances exhibited the highest hardness and the lowest tensile strength, according to the results.

Ajezi-Sardroud et al. investigated methods for enhancing the penetration depth and physical characteristics of the weld zone in aluminum alloy 6061-T6 using active fluxes containing titanium oxide (TiO_2) and silicon oxide (SiO_2) during (TIG) welding. The active fluxes, which ranged in concentration from 2.5% to 10% by weight, were added to the welding process. Mechanical properties were evaluated through micro-Vickers tensile experiments. The results showed that the material with the greatest tensile strength was observed in the base metal, but in the welded samples, the active flux containing 10% TiO_2 produced the greatest tensile strength. The use of titanium active flux resulted in a tensile strength ratio of 90% compared to the mode without flux[23]

Reda, et al investigated the mechanical, thermal, metallurgical and aspects of TIG welding of Ti-6Al-4V alloys. They performed a 3D transient finite element method simulation to predict how welding current influences heat input, weld bead geometry and residual stresses along the weld line. They then validated the FEM simulation by comparing it with experimental data on temperature distribution and weld bead geometry. Finally, they conducted an experimental study to examine the impact of an appropriate range of TIG welding current (130-170 A, as predicted by the FEM simulation) on its microstructure, micro-hardness, and its tensile strength of a 12-mm-thick alloy plate. The experimental results matched well with the FEM simulation data. The researchers discovered that employing a modest weld current of 130A results in a higher tensile strength and greater rigidity of the weld joint due to its lower heat input, higher cooling rate, and finer formation [24].

The purpose of this paper is to weld AA6061-T6 alloy using the Taguchi method and TIG welding procedure parameters. During the welding procedure, process parameters such as (current, speed, and gas flow) were varied. The research involved three major phases. First, a numerical model simulating the Tungsten Inert Gas welding procedure of 6061-T6 aluminum alloy was developed using the Ansys software. A moving heat source was incorporated in the finite element method heat source model to create an accurate simulation of the procedure of arc welding. Second, based on the FEM simulation results, the appropriate welding current range was determined and verified experimentally to validate the simulation by comparing it to experimental temperature measurements and weld bead geometries. Finally, the effects of the welding process on the microstructure and mechanical properties, specifically hardness enhancement, of AA6061-T6 welding joints were studied experimentally. Also performed were analysis of variance (ANOVA), S/N ratio analysis, and regression analysis.

TIG welding is a process with multiple inputs and multiple outputs. To obtain a joint using welding that conforms to the specified parameters, it

is necessary to ascertain the input parameters for every newly welded product. There are numerous Input parameters for TIG welding techniques that significantly influence the integrity of a weld joint. These parameters were determined based on the parameters of the welding machine used in the experiments and previous practical efforts in selecting the best three parameters with two-level and an average third-level value for these parameters that affect the geometry of the weld joint and produce the best welding results. These parameters with levels include welding current of 90A, 95A, 100A, welding speed of 60 mm/min,80 mm/min,100 mm/min, and gas flow rate.The novelty of the work is concentrated on the analysis of variance (ANOVA), S/N ratio analysis, and regression analysis for the executed tests on the welded specimens. And to assist in the fast and inexpensive production of excellent products. The current project focuses on process parameter optimization when welding with a TIG Al6061 alloy.

MATERIALS AND METHOD

The experimental procedure is the set of steps that were followed during the testing and analysis of the (TIG) welding parameters for 6061T6 aluminum alloy. It includes the preparation of the welding samples, the setup of the welding equipment, the selection and adjustment of the welding parameters, and the execution of the welding process as shown in the Figure 1 represent the Welding Machine used in Experimental work and Figure 2. shows TIG Welding line shape formed in the welding sheet of aluminum piece. The procedure also involves the recording of various welding inputs parameters such as welding current, welding speed, gas flow rate, and electrode type. Figure3 shows the shape of the designed welding lines and their butt joints after welding operations. The collected data is then analyzed and evaluated to determine the optimal TIG welding parameters for 6061-T6 aluminum alloy. Clearly demonstrates in Figure 4. Using a mechanical machining process, 6061-T6 aluminum alloy sheets with a thickness of 3 mm were cut to the needed dimensions of 60 × 80 mm for use as the experimental base metal in this analysis. All surfaces are washed to remove oxides, grime, and rust prior to welding. Table 1 and Table 2 demonstrate the mechanical properties and chemical composition of 6061-T6 Aluminum alloys, respectively. For welding alloy 6061-T6 aluminum, ER 4043 welding wire with a 2.5 mm diameter was utilized as filler material. This welding wire, containing 5% silicon, is generally preferred due to its superior flow ability, crack resistance, ease of welding, and aesthetic weld results. However, the suitability of this welding wire depends on the particular application, as it has both advantages and disadvantages. Compared to other wires that are suitable for the same base metal, ER 4043 is less prone to smut formation and crater the cracking, and it exhibits reduced crack sensitivity, making it an ideal choice to avoid stress corrosion cracking. Table 3 displays the results of the chemical examination of the electrode welding.

Fig. 1. Welding tig machine Beam-350 used in experimental work

Fig. 2. TIG welding line shape formed in the welding sheet of aluminum piece

Taguchi's design

The Taguchi process method is a collection of mathematical engineering models. This technique is used for finding the best models [25], saving money and time. Using the MINITAB application, which performs by employing the S/N ratio, and then performing and evaluating the findings. The equation below, written as, [26] displays the (S/N).

$$S/N = -10\log_{10}\left(\frac{1}{n}\sum_{i=1}^{n}\left(\frac{1}{y_i^2}\right)\right) \qquad (1)$$

where: N – refers to the number of observations, *y* refers to data used experimentally. Taguchi L9 in the current work. Orthogonal arrays are used to identify optimal welding parameters. Tables 4 and Table 5 illustrate the details of welding parameters.

The fluorescence of X-rays is a nondestructive technique for determining the elemental composition of alloys, was utilized in the analysis to determine the chemical structure of the metal. By detecting the X-ray fluorescence that a sample triggered by an X-ray source emits, sample chemistry can be ascertained. Each component of the sample emits a unique set of fluorescence from X-rays that is unique to that component. Five samples of base metal were used to measure the mechanical characteristics from the tensile test, and they were compared to the reference sheet.

Temperature distribution in welding sheets by ANSYS method

This study included obtaining the geometry of the three weld areas, especially the melting area, by the thermal distribution represented by the temperatures of all areas in all welds, using the ANSYS program for sheets made of aluminum alloys 6061-T6 in the TIG welding process. It was assumed that the thermal properties of the sheets, filler weld material, and heat affected zone (HAZ) were the same and dependent on temperature. A 3D model of a butt-weld joint of two plates was simulated. The ANSYS Workbench software was utilized to conduct thermal analysis and the temperature distribution in the butt-welding sheets weldments. The triangular surface meshing was selected for the model to obtain better results and transient thermal analysis was conducted for the simulation. Figure 5 presents the geometric representation, and identical mesh of the analyzed work piece, which are significant factors affecting the precision and concourse of)FEM(simulation data results. The element number type, mesh size in various regions, and the density of the mesh also play a crucial role in this regard.

Hardness test

The Vickers hardness test is a non-destructive method used to compute a material's hardness by pressing a diamond indenter into its surface with a specific load and measuring the indentation's size. This provides useful information about a material's resistance to denting and cracking at the microscopic level [29]. Test of (Hv) micro- hardness can be used to find the average Hv of the base metal of AA6061-T6 alloy at approximately

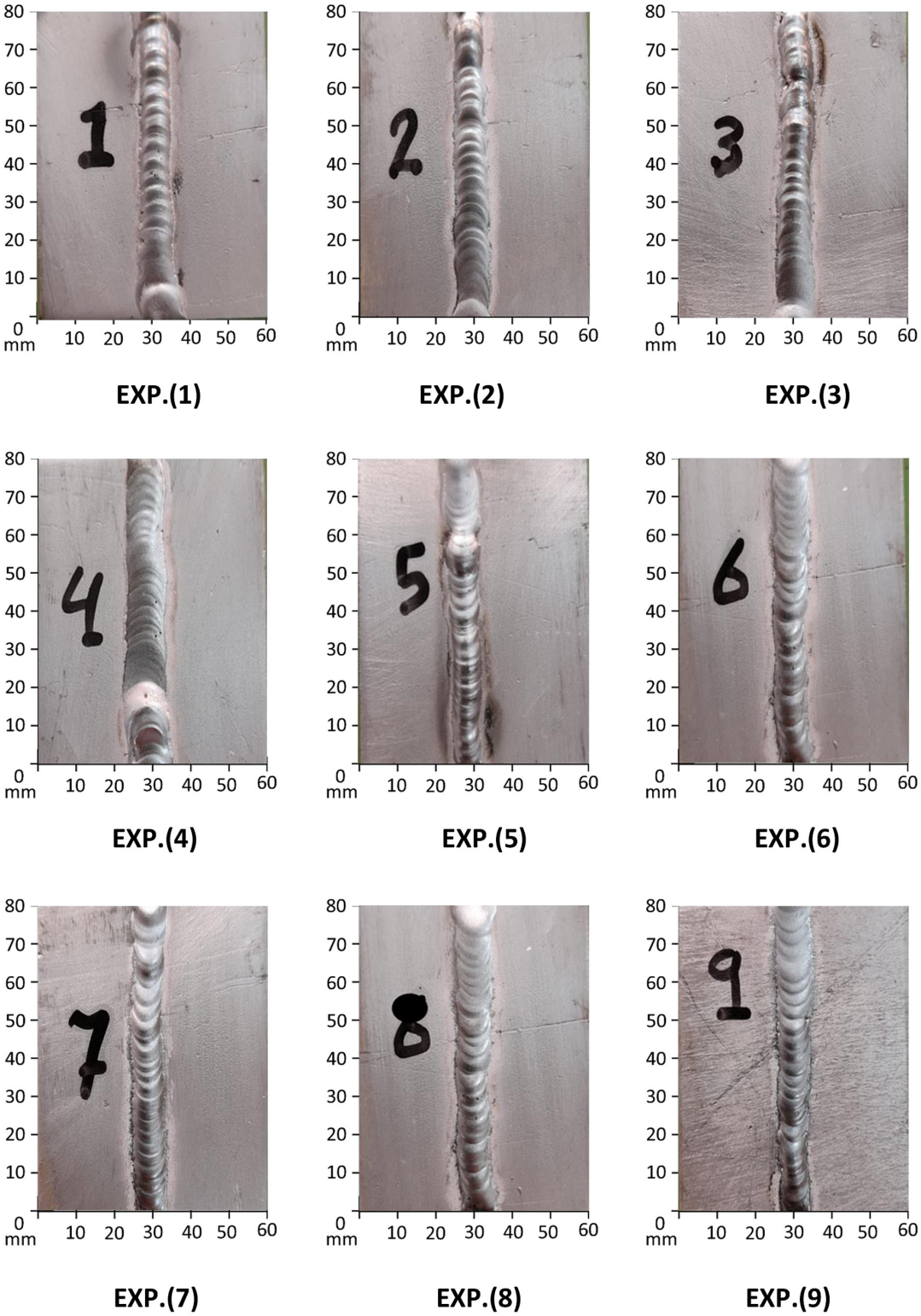

Fig. 3. Butt joints geometries after welding operations

10 points along the cross-sectional centerline of the weld using a micro hardness apparatus. The Hv device is illustrated in Figure 6. The depth of the indentation is typically between 0.01 and 0.1 millimeters, which is quite small as shown in Figure 7.

RESULTS AND DISCUSSIONS

The present study covers TIG welding of AA6061- T6 alloy sheet.The process of welding was performed at different welding parameters (I, v, and *f*) the applicable range of

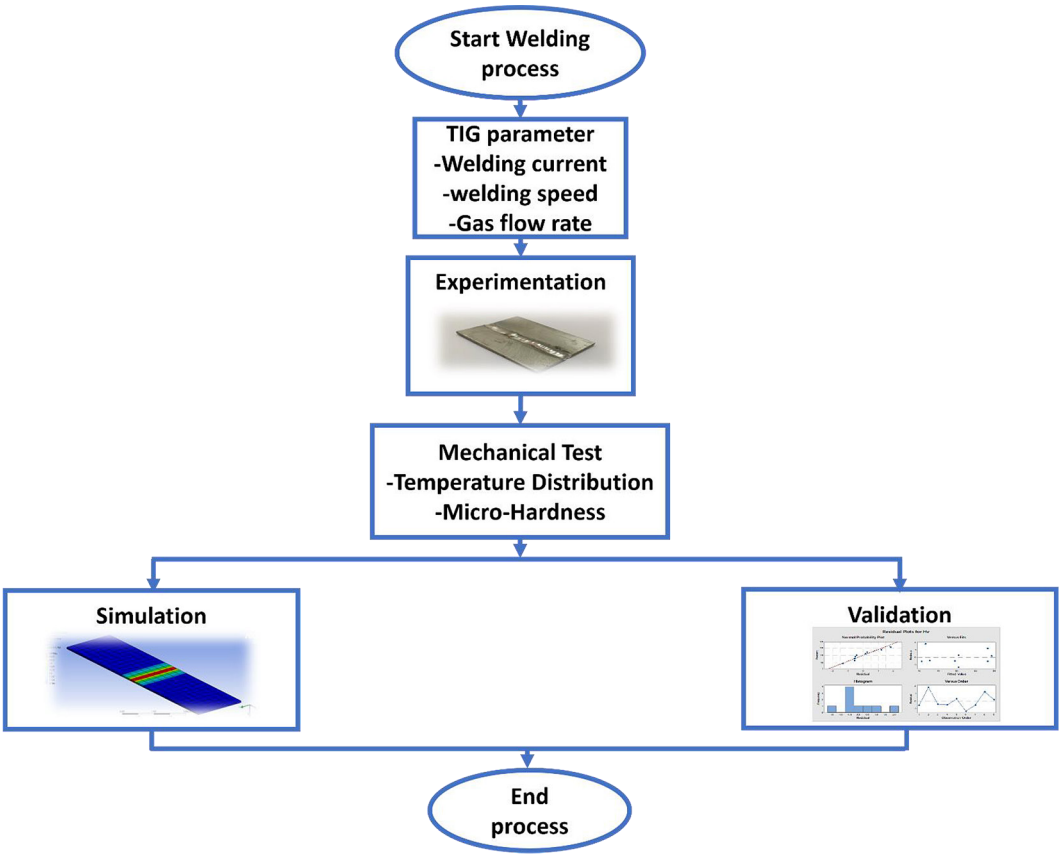

Fig. 4. Experimental flowchart that analyzed and evaluated for 6061-T6 aluminum alloy

Table 1. Chemical composition of Al 6061-T6 alloy sheets

Element %wt	Mg	Si	Cr	Mn	Ti	Cu	Zn	Fe	Al
Standard [27]	0.8–1.2	0.4–0.8	0.04–0.35	Max 0.15	Max 0.15	0.15-0.4	Max 0.25	Max 0.7	Balance
Measured	0.95	0.65	0.068	0.055	0.038	0.34	0.18	0.57	Balance

Table 2. Mechanical properties of Al 6061-T6 alloy sheet

Parameter	Ultimate strength (MPa)	Hardness (HV)	Modulus of elasticity (GPa)
Standard [28]	310	107	68.9
Measured	325.306	105	69.3

Table 3. Chemical Composition of (wt.%) of ER4043 filler material

Material	AL	Si	Mg	Cu	Fe	Mn	Zn	Ti
ER4043	Bal.	5.6	0.05	0.3	0.8	0.05	0.1	0.02

welding process variables was empirically selected according to the FEM results. The results were compared using ANSYS software. The Vickers device was used to evaluate the hardness of the welded joint and determine the optimal hardness determined by the Taguchi method.

Comparison of experimental and FEM results related to temperature distribution

As shown in the Fig. 8 the temperatures distribution in the weld zones of the two jointly welded sheets for nine pieces of 3 mm thick and 80 mm long of Al alloy 6061-T6 as the welding flame moves from the point Z = 0 to

Table 4. Welding parameters with levels

Levels	*I* Amps	V mm/min	*f* L/min
1	90	60	8
2	95	80	9
3	100	100	10

Note: *I* – refer to the welding current, *V* – refers to the welding speed and f refers to the gas flow rate of the welding process.

Table 5. Obtained for the s' L_9 orthogonal array

Experiment No.	I Amps	V mm/min	f L/min
1	90	60	8
2	90	80	9
3	90	100	10
4	95	60	9
5	95	80	10
6	95	100	8
7	100	60	10
8	100	80	8
9	100	100	9

Z = 80 mm in the orientation of weld. FEM simulation was utilized to determine the welding joint geometry, the effect of some welding factors on the geometry, and the obtained results in our current research. Simulations were performed with different welding currents of 90A, 95A and 100A, and the appropriate weld joint geometry and transition temperatures for TIG 6061-T6 welded work pieces for different welding speeds and flow rates were obtained. As shown in Figure 8, the red regions indicate melting zones (FZs) whose melting temperature should be greater than the melting point temperature unit of 680°C for 6061-T6 AA. It was observed that the use of a welding current of 100 A. Fig. 8 resulted in an increase in the temperature at the peak of the free zone. Excessive temperature during welding can negatively impact the microstructure and properties of the material. Based on the FEM simulations conducted, it was determined that the appropriate range of welding currents is between 90A to 100A. The (Q) for TIG welding process is calculated using the equation below [30].

$$Q = \frac{\xi V I}{v} \quad (2)$$

where: Q – the heat input for TIG welding, V – a fixed voltage as (32 volts), I – the welding current, v – welding speed rate, ξ – efficiency.

The heat input compute by using this equation above. The total heat input value per unit length of Welded joints is shown in Table 6 for varying situations. The Q value influences the cooling rate after welding, with the maximum Q resulting in a slower cooling rate [29]. These findings are essential for understanding the resulting mechanical characteristics and microstructures, as discussed later. Through the simulation of the heat cycle during welding, the samples experience heat transfer through conduction, convection, and radiation modes. The Q Q is transmitted first in y-axis and x-axis simultaneously until a steady distribution is achieved. The temperature degree at the. The heat source's front temperature is comparatively lesser than its back temperature [31].

Figure 8 illustrates the Hv profile of the (WZ) welded zone. The diagram clarifies that the hardness is lowered as it approaches to the center of the weld line, as it reaches to its minimum value at 10mm distance from center. In Fig. 8 the distribution of microhardness using various TIG currents. It is evident that the joints' hardness reduced as the TIG current

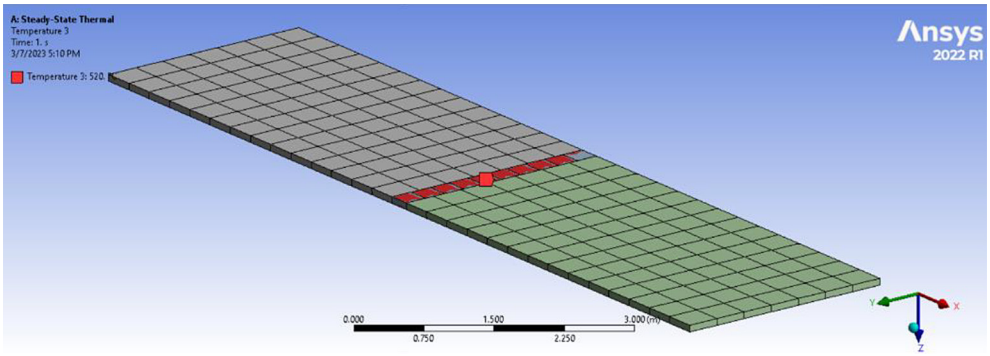

Fig. 5. 3D model of Butt-weld joint after meshing for FEM TIG welding process

Fig. 6. A Vickers hardness (Hv) tester

was increased. In HAZ, the hardness dropped from about 80 HV to 60 HV. The figure demonstrates how the joint's softening area always grew. The PMZ granules became coarser as the heat input increased, lowering the PMZ's hardness. Conduction, convection, and radiation modes of transfer of heat are all applied to the workpiece during the modeling of the welded thermal cycle. the transfer of the Heat is introduced in two directions – first in the thickness (y-axis) and subsequently in the width (x-axis) directions – until uniform distributions are attained. The rear of the heat source has a temperature gradient that is comparatively greater than the front of the source [32].

Results of hardness

The aluminum weld joint is heated by heat during the welding process, and then swiftly cooled. This change in the rate of heating and cooling affects the microstructure and mechanical properties of aluminum, and in turn changes the hardness of the weld area. The speed of cooling leads to the emergence of granules of different sizes. Smaller and more brittle microstructures, which can lead to reduced toughness. The specific hardness distribution of a TIG weld depends on a number of variables, such as welding parameters, the properties of the weld material, and the cooling rate of the weld metal. With these variables, it is very important to control these variables carefully to obtain the correct hardness and mechanical properties of the final product. The Vicker hardness tester device was utilized to determine the hardness of nine workpieces. Every single workpiece underwent a hardness test at seven predetermined locations: the center, the left and right sides of the HAZ, and the base metal zone.as shown below in Table 7

For the initial three samples are depicted in Fig. 8a. It is noted that in the base metal zone, the micro-hardness increases with the welding current and reaches its maximum limit of approximately, a distance of 30 mm to the right and left of the specimen, before decreasing with the welding current as it approaches the heat-affected zone at a distance of 10mm to the right and left of the specimen. And it begins to rise again in the midsection of the aluminum specimen in the welding area. In the same previous pattern for samples (4, 5, and 6) shown in Fig. 8b, the micro-hardness in the base metal region increases with the welding current until it reaches its maximum value near 30mm, after which it begins to decrease with the welding current decrease. The microhardness begins to increase

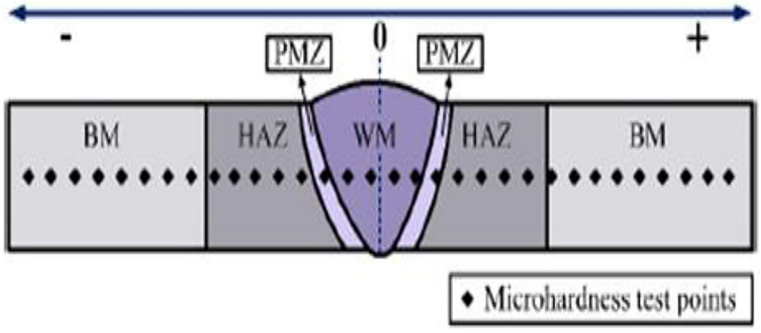

Fig. 7. Microhardness welding regions test points

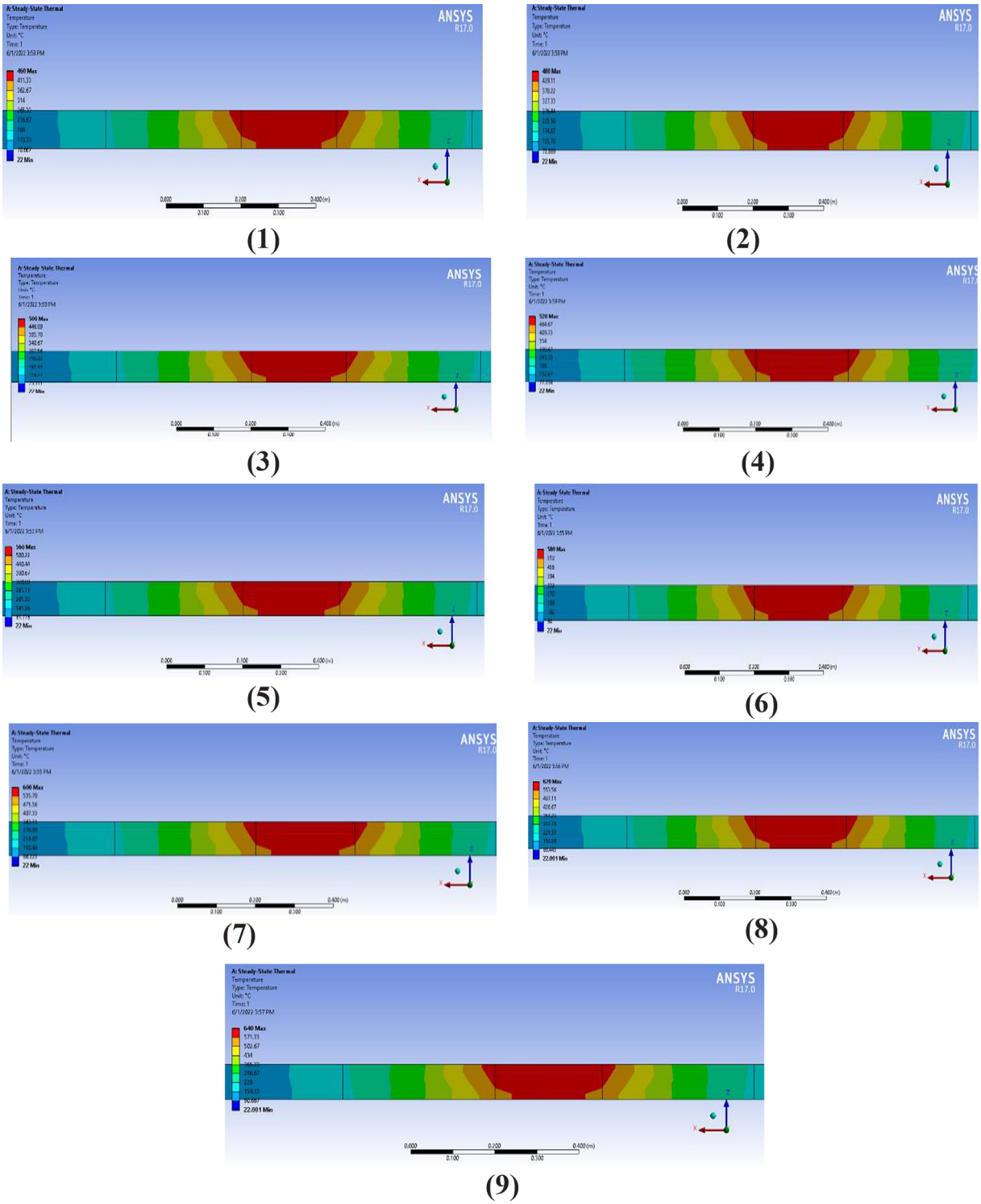

Fig. 8. Thermal simulation the temperatures weld joint shapes by fusion welding process for nine weldments

in the middle as the welding current increases [33, 34]. Finally, the last three specimens (7, 8, 9) that elucidate in Figure (8-c). The microscopic firmness similar to previous instances, the micro-hardness is directly proportional to the welding current, at the base metal zone the micro-hardness reaches its utmost value. At a distance of approximately 10 mm, the micro-hardness in the heat-affected zone begins to decrease. With an increase in the welding current at the center of the specimens' weld zone, the microhardness increases once more.

Table 6. The amount of heat applied during welding was determined for different levels of welding parameters

Experiment No.	I, A	V, mm/min	f, l/min	Q, J/mm
1	90	60	8	38.4
2	90	80	9	28.8
3	90	100	10	23.04
4	95	60	9	40.53
5	95	80	10	30.4
6	95	100	8	24.32
7	100	60	10	42.666
8	100	80	8	32
9	100	100	9	25.6

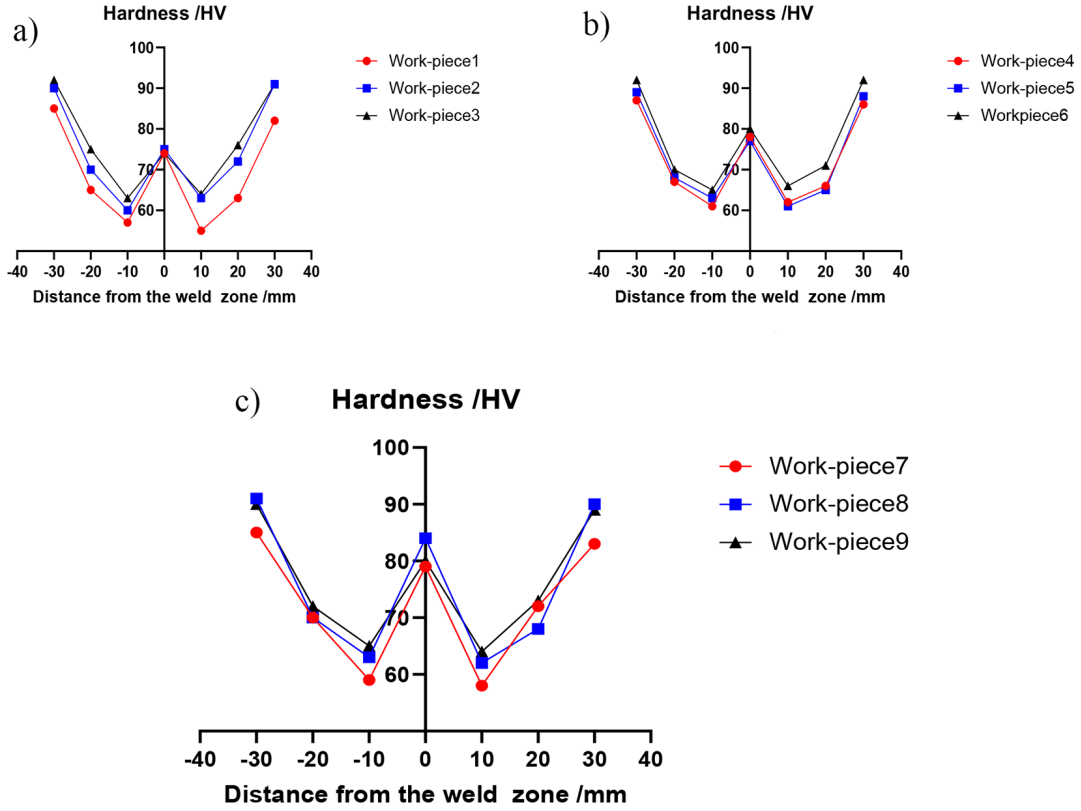

Fig. 9. Distribution of micro-hardness using various TIG currents for nine workpieces: (a) hardness test for workpiece (1, 2, 3); (b) hardness tests for work-piece (4, 5, 6); (c) hardness tests for workpiece (7, 8, 9)

Investigation of the micro-hardness (HV) parameter results using Taguchi

When aluminum 6061-T6 is welded, the heat input can cause changes in the microstructure of the metal. It may have an impact on how the material behaves mechanically, including changes in Hv. A number of variables, such as the welding speed, current, and gas flow rate both during and after welding, can affect the Hv of the welding zone. To determine the optimal level of each parameter for maximizing the reaction that affects Hv on a Aluminum workpiece, (S/N) ratio is used as a measure of the accuracy of the output. In general, a higher S/N ratio indicates a better output quality. S/N ratio and mean are shown in Table 8, Table 9 and Table 10, respectively [35]. Table 8 and Table 9 illustrate the results of S/N ratio and mean values of all parameters are consistent with each other. By choosing the larger number, no prediction is required. The plot of the main effects for both means and S/N ratio is shown in Figure 10 and Figure 11 respectively. A combination of parameters reached to the

Table 7. Measuring the hardness of workpieces (WP) at different distances

Distance /mm	Hardness /HV								
	WP1	WP2	WP3	WP4	WP5	WP6	WP7	WP8	WP9
-30	85.21	90.25	92.54	87.65	89.24	92.01	85	91	90
-20	65.75	70.47	75.24	67.27	68.35	70.14	70.98	70.14	72.05
-10	57.01	60.56	63.78	61.04	63.34	65.94	59.14	63.72	65.16
0	75.65	75.65	75.65	75.65	75.65	75.65	75.65	75.65	75.65
30	55.01	63.26	64.55	62.04	61.46	66.75	58.16	62.09	64.47
20	63.01	72.48	76.75	66.65	65.24	71.14	72.05	68.10	73.25
10	82.45	91.02	91.24	86.04	88.16	92.08	83.07	90.47	89.51

Table 8. The Hv mean and S/N ratio's values

Experiment	I Amps	V mm/min	f L/min	Hv in HAZ	S/N ratio	Mean
NUM.	X1	X2	X3	Hv	SNRA1	MEAN1
1	90	60	8	75.65	37.5762	75.65
2	90	80	9	78.45	37.8919	78.45
3	90	100	10	76.65	37.6902	76.65
4	95	60	9	79.25	37.9800	79.25
5	95	80	10	80.45	38.1105	80.45
6	95	100	8	78.82	37.9327	78.82
7	100	60	10	82.75	38.3554	82.75
8	100	80	8	84.47	38.5340	84.47
9	100	100	9	83.85	38.4701	83.85
Conformation test	100	80	9			

Table 9. Table of responses for the signal-to-noise ratio for (Hv)

Level	I Amps	V mm/min	f L/min
1	37.72	37.97	38.05
2	38.04	38.18	38.11
3	38.45	38.07	38.05
Delta	0.73	0.21	0.06
Rank	1	2	3

Table 10. Responses for mean for (Hv)

Level	X1	X2	X3
1	76.92	79.22	79.98
2	79.84	81.12	80.52
3	83.69	80.11	79.95
Delta	6.77	1.91	0.57
Rank	1	2	3

greatest hardness value (Hv). The ideal parameters for the highest S/N ratio are found by using welding current X1 of 100A, welding speed X2 of 80mm/min, and gas flow rate X3 of 9 l/min. The optimal level ($X1_3$, $X2_3$, $X3_3$) is not founded in the nine experiments which are not included in the nine experiments as shown previously in Table 6. That was carried out utilizing Taguchi orthogonal array. It's essential to keep in mind that the Taguchi orthogonal array only includes a small subset of all potential tests. (81 experiments in total, given four parameters with three levels each).

ANOVA technique for the change in micro-hardness in the heat effected zone

The ANOVA test is a statistical method that calculates the percentage of contribution (P%) of each parameter, such as welding speed, current, to the outcome. Table 11 shows that the first criterion, Hv, was analyzed using ANOVA. From Table 11 the impact of the parameters on the hardness in the (HAZ) can be observed, with the (I) having the most significant effect, followed by the (V). This indicates that these two parameters have a greater influence on micro-hardness than the gas flow rate. The equation for the regression model

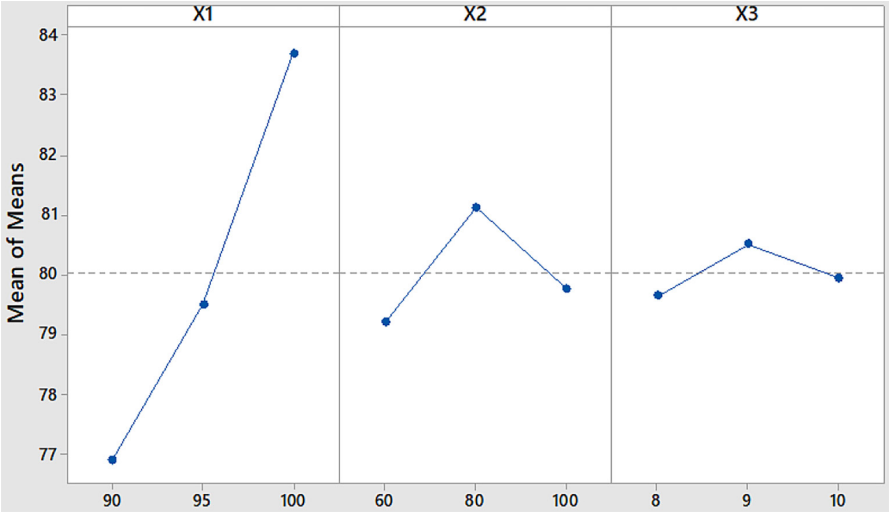

Fig. 10. Principal effect diagram for mean micro hardness (Hv)

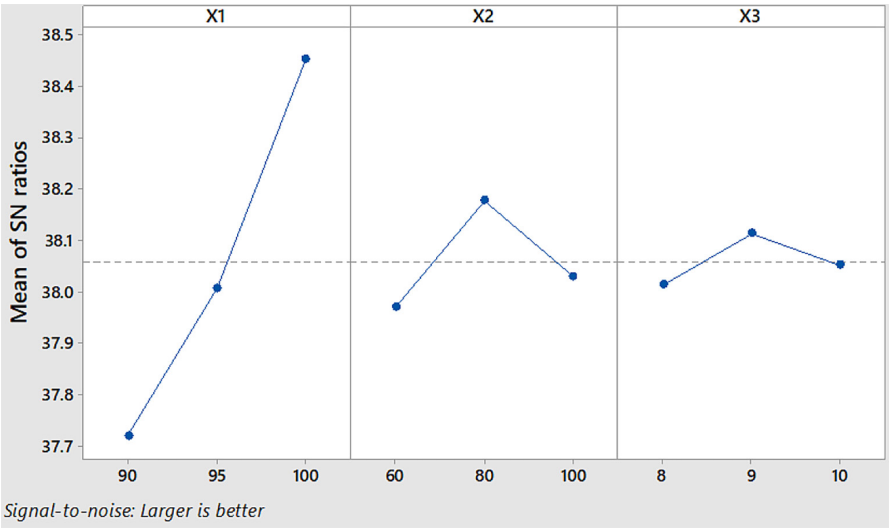

Fig. 11. Principal effect diagram for S/N ratio micro hardness (Hv).

Table 11. Analysis of variance (ANOVA) for micro-hardness

Source	DF	Seq SS	Contribution	Adj SS	Adj MS	F-Value	P-Value
X1	2	70.0864	90.95%	70.0864	35.0432	2076.29	0.000
X2	2	5.7678	7.48%	5.7678	2.8839	170.87	0.006
X3	2	1.1700	1.52%	1.1700	0.5850	34.66	0.028
Error	2	0.0338	0.04%	0.0338	0.0169		
Total	8	77.0580	100.00%				

of Hv eq. (3) was derived using Minitab software. This equation predicts the expected outcome of the nine experiments.

$$Hv = 13.2 + 0.677\ X1 + 0.0139\ X2 + 0.152\ X3 \quad (3)$$

$$\text{R-sq} = 90.09\%$$

where: R-square – the determination coefficient

CONCLUSIONS

According to the aforementioned conclusions, it can be said that the impact of various welding parameters on the mechanical characteristics as well defects in welding of AA6061-T6 using ER4043 filler metal by employing TIG welding

can be summed up as follows: the thermal and mechanical effects of a movable heat source of TIG were predicted and studied using finite element analysis & experimental testing of 6061-T6 alloy plate welding. Both the experimental and FEM simulation results show that there are meaningful correlations among the welding current & weld joint properties.The welding current that will result in the least amount of residual stresses on the material during welding is chosen for the given parameters using the thermal model. This makes it possible to enhance the TIG welding procedure by maximizing the welding current. The weld bead geometry and projected temperature distribution along the welding line at various welding current of experimentally TIG welded connections are in great agreement, according to FEM results. The fusion zone showed higher hardness of the weld metal compared to the HAZ and BM regions, where high hardness was obtained in the welding area. The greatest hardness is 84.9 HV in the WZ and in the original metal its value is 69.1 HV.

It has been found that the highest hardness value realized at the welding current value of 210 amperes, the speed mm/min, and the shielding gas flow rate of 10 liters/min (workpiece 8). S/N ratio as well as ANOVA results revealed that current, following speed and gas flow rate, had the largest impact on HAZ hardness. The developed model is more effective at predicting the micro hardness for welded specimens through correlating with process parameters, according to regression analysis. The estimated error among the model & the experimental results is 4.0% or less and R^2=90.09%. This shows that the created regression equation model is more effective at making predictions.

In order to obtain adequate weld penetration and tensile properties to meet the service requirements of thin-walled parts, these welding process factors must be considered, in addition to the current used to weld, such as welding speed, flow of gas rates, as well as other influencing variables involving welding orientation, heat source parameters, etc., should be carefully considered and optimized. The response relationship between mechanical features, and the microstructure variation will also be the focus of additional research from a quantitative standpoint. This will improve the mechanical characteristics of the butt joint and serve as a theoretical foundation for the future welding of thin-walled parts.

REFERENCES

1. Fortain J.M., Gadrey S. How to select a suitable shielding gas to improve the performance of MIG and TIG welding of aluminium alloys. Welding International. 2013; 27(12): 936–947. doi: 10.1080/09507116.2012.753257.
2. Mutombo K., M. du Toit. Corrosion fatigue behaviour of aluminium alloy 6061-T651 welded using fully automatic gas metal arc welding and ER5183 filler alloy. Int J Fatigue. 2011; 33(12): 1539–1547. doi: 10.1016/j.ijfatigue.2011.06.012.
3. Ramanaiah N., Prasad Rao K. Effect of modified AA4043 filler on corrosion behavior of AA6061 alloy GTA welds. International Journal of Advanced Manufacturing Technology. 2013; 64: 9–12, 1545–1554. doi: 10.1007/S00170-012-4121-4.
4. A.A.-A.-K.E. Journal and undefined 2019. Modeling of Bending Properties of Stainless Steel 304 Sheets Welded by Tungsten Inert Gas Welding Process. Iasj.Net. 2019; 15(4): 10–22. doi: 10.22153/kej.2019.09.003.
5. Zhao Y., Yang Z., Domblesky J., Han J., Z.L. Investigation of through thickness microstructure and mechanical properties in friction stir welded 7N01 aluminum alloy plate. Materials Science and Engineering: A. 2019; 760: 316–327. Accessed: Jul. 31, 2023. [Online]. https://www.sciencedirect.com/science/article/pii/S0921509319307798
6. Cetkin E., Çelik Y. Microstructure and mechanical properties of AA7075/AA5182 jointed by FSW. J Mater Process Technol. 2019; 268: 107–116. Accessed: Jul. 31, 2023. [Online]. https://www.sciencedirect.com/science/article/pii/S0924013619300056
7. Salih O., Neate N., Ou H., W.S.-J. of M. Processing, and undefined 2020. Influence of process parameters on the microstructural evolution and mechanical characterisations of friction stir welded Al-Mg-Si alloy. J Mater Process Technol. 2020; 275: 116–366. Accessed: Jul. 31, 2023. [Online]. https://www.sciencedirect.com/science/article/pii/S0924013619303383
8. Wang Z., Zhang Z., Xue P., Ni D., Z. M.-M. S. and, and undefined 2022. Defect formation, microstructure evolution, and mechanical properties of bobbin tool friction–stir welded 2219-T8 alloy. Materials Science and Engineering. 2022; A(832): 142–414. Accessed: Jul. 31, 2023. [Online]. https://www.sciencedirect.com/science/article/pii/S0921509321016786
9. Sasikumar A., Gopi S., Mohan D.G. Prediction of Filler Added Friction Stir Welding Parameters for Improving Corrosion Resistance of Dissimilar Aluminium Alloys 5052 and 6082 Joints. Advances in Materials Science. 2022; 22(3): 79–95. doi: 10.2478/ADMS-2022-0014.

10. Kulkarni A., Dwivedi D., M.V. and, and undefined 2020, Microstructure and mechanical properties of A-TIG welded AISI 316L SS-Alloy 800 dissimilar metal joint. Materials Science and Engineering: A. 2020; 790: 139–685. Accessed: Jul. 31, 2023. [Online]. https://www.sciencedirect.com/science/article/pii/S0921509320307644
11. Chen L., Wang C., Xiong L., X. Zhang, G.M.-M. & Design, and undefined 2020. Microstructural, porosity and mechanical properties of lap joint laser welding for 5182 and 6061 dissimilar aluminum alloys under different place. Elsevier, Accessed: Jul. 31, 2023. [Online]. https://www.sciencedirect.com/science/article/pii/S0264127520301593
12. Wang H., Liu X., and undefined 2020. Research on laser-TIG hybrid welding of 6061-T6 aluminum alloys joint and post heat treatment. Metals (Basel). 2020; 10: 130–145. doi: 10.3390/met10010130.
13. Li L., Wang S., Huang W., and undefined 2020. Microstructure and mechanical properties of electron beam welded TC4/TA7 dissimilar titanium alloy joint. J Manuf Process. 2020; 50: 295–304. Accessed: Jul. 31, 2023. [Online]. Available: https://www.sciencedirect.com/science/article/pii/S1526612519303883
14. Mohanavel V., Ravichandran M., S.K.-M.T. Proceedings, and undefined 2018, Optimization of tungsten inert gas welding parameters to: Attain maximum impact strength in AA6061 alloy joints using Taguchi Technique. Elsevier, Accessed: Jun. 21, 2023. [Online]. Available: https://www.sciencedirect.com/science/article/pii/S2214785318326166
15. Jayashree P., Sharma S., Shetty R., A.M.-M. today, and undefined 2018. Optimization of TIG welding parameters for 6061Al alloy using Taguchi's design of experiments. Elsevier, Accessed: Jun. 21, 2023. [Online]. https://www.sciencedirect.com/science/article/pii/S2214785318324490
16. Sathish T., Tharmalingam S. V.M.-A. in M., and undefined 2021. Weldability investigation and optimization of process variables for TIG-welded aluminium alloy (AA 8006). *hindawi.com*, Accessed: Jun. 21, 2023. [Online]. Available: https://www.hindawi.com/journals/amse/2021/2816338/
17. Moshi A.A.M., Ravindran D., Sundara Bharathi S.R., Rex F.M.T., Kumar P.R. TIG Welding Process Parameter Optimization for Aluminium Alloy 6061 Using Grey Relational Analysis and Regression Equations. Advances in Intelligent Systems and Computing. 2020; 979: 413–425. doi: 10.1007/978-981-15-3215-3_41.
18. Bansal A., Kumar M., Shekhar I., S.C.-M.T., and undefined 2021. Effect of welding parameter on mechanical properties of TIG welded AA6061. Elsevier, Accessed: Jun. 21, 2023. [Online]. Available: https://www.sciencedirect.com/science/article/pii/S2214785320356820
19. Adalarasan R., Santhanakumar M. Parameter Design in Fusion Welding of AA 6061 Aluminium Alloy using Desirability Grey Relational Analysis (DGRA) Method. Journal of The Institution of Engineers (India): Series C. 2015; 96(1): 57–63. doi: 10.1007/S40032-014-0128-Y.
20. Khoshroyan A., A.D.-T. of N.M.S. of, and undefined 2020. Effects of welding parameters and welding sequence on residual stress and distortion in Al6061-T6 aluminum alloy for T-shaped welded joint. Elsevier, Accessed: Jun. 21, 2023. [Online]. https://www.sciencedirect.com/science/article/pii/S1003632619651812
21. Tolephih M., Mashloosh K., Z.W.-A. engineering journal, and undefined 2011. Comparative study of the mechanical properties of (FS) and MIG welded joint in (AA7020-T6) aluminum alloy," iasj.netMH Tolephih, KM Mashloosh, Z WaheedAl-khwarizmi engineering journal. 2011; 7(2): 35: 2011. Accessed: Aug. 01, 2023. [Online]. https://www.iasj.net/iasj/download/98f8bf9593622e23
22. Jayashree P., Gowrishankar M., S.S.-J. of M., and undefined 2020. Influence of homogenization and aging on tensile strength and fracture behavior of TIG welded Al6061-SiC composites. Elsevier, Accessed: Jun. 21, 2023. [Online]. Available: https://www.sciencedirect.com/science/article/pii/S2238785420301083
23. Ajezi-Sardroud R., Mostafapour A., F. A.-S.-I. J. of, and undefined 2022. Effect of Active Flux on Aluminum 6061 and its Mechanical Properties by Gas Tungsten Arc Welding Process. 2022; 35(8), 1501–1508. doi: 10.5829/ije.2022.35.08b.06.
24. Reda R., Magdy M., M.R.-I.J. of S. and Technology, and undefined 2020. Ti–6Al–4V TIG weld analysis using FEM simulation and experimental characterization. Springer. 2019; 44(3): 765–782. doi: 10.1007/s40997-019-00287-y.
25. Aghdeab S.H., Ghazi Abdulameer A., Hussein Kashkool L., Rasim Mohammed A. Optimization the Effect of Electrode Material Change on EDM Process Performance Using Taguchi Method. iasj.netSH Aghdeab, AG Abdulameer, LH Abdulameer, AR MohammedAl-Khwarizmi Engineering Journal. 2020; 16(1). doi: 10.22153/kej.2020.09.001.
26. Mondolfo L. Aluminum alloys: structure and properties. 2013. Accessed: Jul. 31, 2023. [Online]. https://books.google.com/books?hl=en&lr=&id=Xf4kBQAAQBAJ&oi=fnd&pg=PP1&dq=Mondolfo,+L.+F.+(2013).+Aluminum+alloys:+structure+and+properties.+Elsevier.%E2%80%8F+&ots=Q66t1rJwuk&sig=aydMm4VrAtnMBj-4v3Pj68yhuGc
27. Alloys W. International Alloy Designations and Chemical Composition Limits for Wrought Aluminum. Wrought Aluminum. 2015. Accessed: Jun. 21,

2023. [Online]. https://www.aluminum.org/sites/default/files/2021-10/Teal%20Sheet.pdf

28. Engineering A.-K., Al J., Jebbur A.M., Alkareem S.S.A., Mustafa F.F. Effect of MIG Welding Parameters on the Mechanical Properties of AISI 304 Austenitic Stainless Steels. 2022; 18(1): 1–15. DOI: 10.22153/kej.2022.01.001.
29. Esmaily M., Mortazavi S., Todehfalah P., M.R.-M. Design, and undefined 2013. Microstructural characterization and formation of α′ martensite phase in Ti–6Al–4V alloy butt joints produced by friction stir and gas tungsten arc welding processes Elsevier. Accessed: Jun. 21, 2023. [Online] https://www.sciencedirect.com/science/article/pii/S026130691200845X
30. Yadaiah N., S.B.-I. international, and undefined 2012. Effect of heat source parameters in thermal and mechanical analysis of linear GTA welding process. 2012; 52(11): 2069–2075. doi: 10.2355/isijinternational.52.2069.
31. Fu G., Lourenco M., Duan M., S.E.-J. of C. Steel, and undefined 2014. Effect of boundary conditions on residual stress and distortion in T-joint welds. Elsevier. 2023. [Online]. Available: https://www.sciencedirect.com/science/article/pii/S0143974X14001977
32. Chennaiah M., P.K., and undefined 2015. Effect of pulsed TIG welding parameters on the microstructure and micro-hardness of AA6061 joints. 2015; 4(4): 182. doi: 10.4172/2169-0022.1000182
33. Ibrahim I., Mohamat S., Amir A., and undefined 2012. The Effect of Gas Metal Arc Welding (GMAW) processes on different welding parameters. Procedia Eng. 2012; 41: 1502–1506. Accessed: Jul. 31, 2023. [Online] https://www.sciencedirect.com/science/article/pii/S1877705812027427
34. Liang Y., Shen J., Hu S., Wang H. Effect of TIG current on microstructural and mechanical properties of 6061-T6 aluminium alloy joints by TIG–CMT hybrid welding. J Mater Process Technol. 2018; 255: 161–174. Accessed: Jul. 31, 2023. [Online]. https://www.sciencedirect.com/science/article/pii/S0924013617305897
35. Datta S., Raza M.S., Das A.K., Saha P., Pratihar D.K. Laser beam welding of NiTinol sheets in butt joint arrangement and optimization of the process using desirability function analysis and metaheuristic techniques. Proceedings of the Institution of Mechanical Engineers, Part E: Journal of Process Mechanical Engineering. 2022. doi: 10.1177/09544089221144509.